Publication Year	2015
Acceptance in OA@INAF	2020-04-16T15:36:02Z
Title	No Evidence of Mass Segregation in the Low-mass Galactic Globular Cluster NGC 6101
Authors	Dalessandro, Emanuele; Ferraro, F. R.; Massari, D.; Lanzoni, B.; Miocchi, P.; et al.
DOI	10.1088/0004-637X/810/1/40
Handle	http://hdl.handle.net/20.500.12386/24077
Journal	THE ASTROPHYSICAL JOURNAL
Number	810

The Astrophysical Journal, 810:40 (11pp), 2015 September 1 doi:10.1088/0004-637X/810/1/40
© 2015. The American Astronomical Society. All rights reserved.

NO EVIDENCE OF MASS SEGREGATION IN THE LOW-MASS GALACTIC GLOBULAR CLUSTER NGC 6101*

E. Dalessandro[1], F. R. Ferraro[1], D. Massari[2,3], B. Lanzoni[1], P. Miocchi[1], and G. Beccari[4]
[1] Dipartimento di Astronomia, Università degli Studi di Bologna, via Ranzani 1, I-40127, Bologna, Italy
[2] INAF—Osservatorio Astronomico di Bologna, via Ranzani 1, I-40127, Bologna, Italy
[3] Kapteyn Astronomical Institute, University of Groningen, P.O. Box 800, 9700 AV Groningen, The Netherlands
[4] European Southern Observatory, Karl Schwarzschild Strasse 2, D-85748, Garching bei Munchen, Germany
Received 2015 April 30; accepted 2015 July 14; published 2015 August 27

ABSTRACT

We used a combination of *Hubble Space Telescope* and ground-based data to probe the dynamical state of the low-mass Galactic globular cluster NGC 6101. We have rederived the structural parameters of the cluster by using star counts and we find that it is about three times more extended than thought before. By using three different indicators, namely the radial distribution of blue straggler stars (BSSs), that of main-sequence binaries, and the luminosity (mass) function, we demonstrated that NGC 6101 shows no evidence of mass segregation, even in the innermost regions. Indeed, both the BSS and the binary radial distributions fully resemble those of any other cluster population. In addition, the slope of the luminosity (mass) function does not change with the distance, as expected for non-relaxed stellar systems. NGC 6101 is one of the few globulars where the absence of mass segregation has been observed so far. This result provides additional support for the use of the "dynamical clock" calibrated on the radial distribution of the blue stragglers as a powerful indicator of the cluster dynamical age.

Key words: binaries: general – blue stragglers – globular clusters: individual (NGC 6101)

1. INTRODUCTION

Globular clusters (GCs) are the most populous, old, and dense stellar aggregates in the Galaxy. They are formed by millions of stars, whose age, distance, and chemical composition can be determined with great accuracy. For this reason, GCs play a crucial role in the current understanding of stellar and dynamical evolution and they represent the ideal target to constrain the interplay between the "environment" and the evolution of stars.

The average age of Galactic GCs (GGCs; $\langle t \rangle \sim 12$ Gyr) is typically significantly larger than the timescales in which the internal dynamical processes occur (Meylan & Heggie 1997). During their evolution, GCs can survive the early expansion triggered by primordial gas expulsion and mass loss due to stellar evolution. Then, their evolution is mainly driven by two-body relaxation, thus reaching higher central concentrations and eventually the core collapse, while loosing stars through the boundary set by the tidal field of their host galaxy (see, for example, Heggie & Hut 2003).

Two-body relaxation drives the long-term dynamical evolution of GCs. Because of this physical process, heavier objects tend to sink toward the cluster centers (mass segregation), while less massive stars are forced toward more external orbits. The typical timescale in which two-body relaxation occurs scales with the number of stars (Spitzer 1987) and it is typically of the order of 1–2 Gyr in GCs (Meylan & Heggie 1997). The internal dynamics of stellar aggregates affect objects of any mass and it can be efficiently probed by means of massive test particles, like blue straggler stars (BSSs), binaries and millisecond pulsars (e.g., Ferraro et al. 2001, 2003). Among them, BSSs have been successfully used for this purpose, since they are numerous and relatively easy to measure. Indeed, Ferraro et al. (2012) have shown that the BSS radial distribution can be efficiently used to rank clusters according to their dynamical age. Using this approach, evidence of mass segregation has been observed in all GCs studied so far, with very few exceptions: ω Centauri, NGC 2419, Palomar 14, Terzan 8, and Arp 2, for which the BSS radial distribution has been found to be indistinguishable from that of any other population (Ferraro et al. 2006a; Dalessandro et al. 2008b; Beccari et al. 2011; Salinas et al. 2012). In general, for clusters that have not reached relaxation yet, the radial distribution of stars of any mass is expected to be the same (apart from possible primordial dissimilarities). The lack of mass segregation in NGC 2419 has been confirmed by Bellazzini et al. (2012), by studying the radial variation of the luminosity function (LF) of main-sequence (MS) stars at different radii,[5] while it has been questioned for Palomar 14 by Frank et al. (2014), who observed an increase of the slope of the stellar mass function (MF) for increasing distance from the cluster center, as expected for relaxed systems.

As part of a large observational campaign aimed at deriving the binary fraction in the external regions of GGCs, we present results about the dynamical state of the low-mass ($M_V = -6.94$; Harris 1996–2010 edition) GC NGC 6101. This is an old ($t \sim 13$ Gyr, Dotter et al. 2010), metal-poor ([Fe/H] $= -1.98$; Carretta et al. 2009) Galactic halo GC, with a low concentration ($c = 0.80$; Harris 1996). A recent analysis of its RR Lyrae content (Cohen et al. 2011) revealed that NGC 6101 is an Oosterhoff type II cluster. This is consistent with the metallicity of the cluster, but it is unusual for its kinematical properties. In fact NGC 6101 is one of the very few metal-poor GCs in the Galaxy with a retrograde motion. Because of its peculiar kinematical properties, it has been possibly connected (Martin et al. 2004) to the Canis Major dwarf galaxy. The stellar content of NGC 6101 has been studied by Sarajedini &

* Based on observations collected at the the Very Large Telescope of the European Southern Observatory, Cerro Paranal, Chile (under proposal 091.D-0562). Also based on observations with the NASA/ESA *HST* (Prop. 10775), obtained at the Space Telescope Science Institute, which is operated by AURA, Inc., under NASA contract NAS5-26555.

[5] The same result has been obtained by Baumgardt et al. (2009), who performed detailed comparison between velocity dispersion profiles and theoretical models.

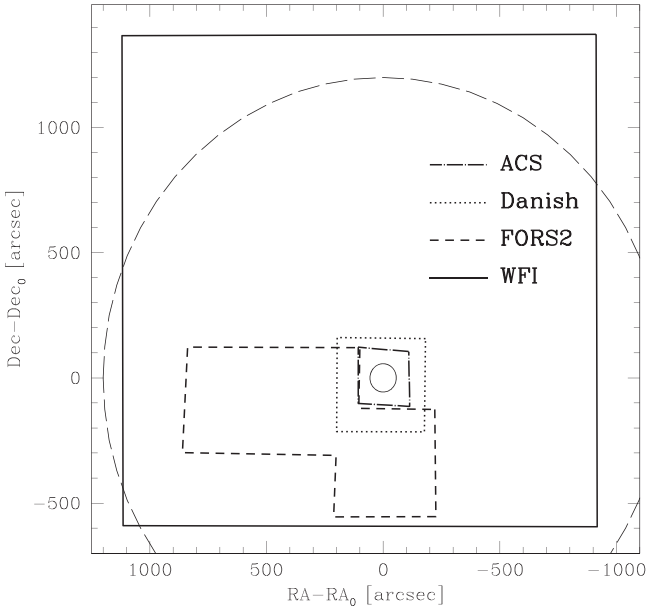

Figure 1. Schematic map of the entire database used in this work with respect to the position of the center of the cluster. The solid and dashed circles represent the cluster core and tidal radii, respectively.

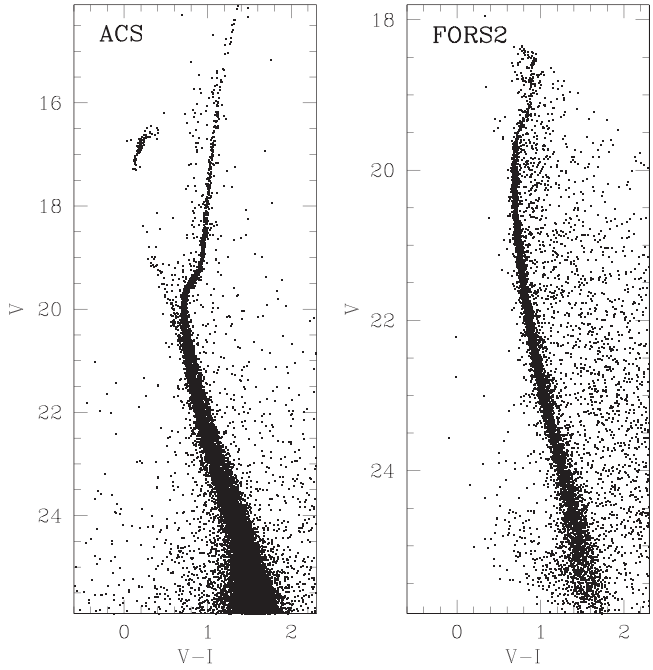

Figure 2. (V, $V-I$) CMDs of the ACS and FORS2 data sets (Section 2).

Da Costa (1991) and later on by Marconi et al. (2001; hereafter M01). In particular, M01 performed a detailed analysis of the radial distributions of different stellar populations of NGC 6101. They found that horizontal branch (HB) stars and BSSs are more centrally concentrated than MS-turnoff stars. They interpreted this behavior as evidence of mass segregation among different populations.

In this study, we investigate the dynamical state of NGC 6101 by using three diagnostics: the radial distribution of (i) BSSs, (ii) MS binaries, and (iii) genuine MS stars with different masses. According to these three indicators, and at odds with the results of M01, we find that NGC 6101 does not show evidence of mass segregation. We compare this observational fact with theoretical expectations and the new dynamical timescale estimates obtained from the newly derived structural parameters.

The paper is structured as follows. In Section 2, we present the details of our observations and the adopted data reduction procedures. In Section 3, we derive the main structural parameters of the cluster. In Section 4, the BSS radial distribution is analyzed and compared to that of the reference populations. In Section 5, we study the binary content of NGC 6101 at different distances from the center. In Section 6, we analyze the radial variations of the luminosity and MF of MS stars. The main results of the paper are summarized and discussed in Section 7.

2. OBSERVATIONS AND DATA ANALYSIS

The data set used in this paper consists of a combination of images obtained with both the *Hubble Space Telescope* (*HST*) and ground-based facilities (see Figure 1).

For the analysis of the BSS radial distribution (see Section 4), we used two publicly available catalogs. The first is the *HST* Advanced Camera for Survey/Wide Field Camera (ACS/WFC) catalog published by Sarajedini et al. (2007; see also Anderson et al. 2008) in the context of the "ACS Survey of Galactic Globular Clusters." This catalog samples the innermost $\sim 120''$ of the cluster. We will refer to this sample as the ACS data set. The (V, $V-I$) color–magnitude diagram (CMD) obtained by using the Johnson–Cousin $V_{\rm ground}$ and $I_{\rm ground}$ magnitudes is shown in Figure 2. The second public data set used in this work consists of the B, V, and I catalog published and fully described by M01 and obtained with the 1.54 mt Danish telescope at ESO/La Silla. In the following, we will refer to this sample as the Danish sample. The corresponding CMD is shown in Figure 3.

The binary fraction analysis (Section 5) has been performed by using deep $V_{\rm HIGH}$ and $I_{\rm BESSEL}$ images obtained with the FORS2 at the Very Large Telescope (Prop ID: 091.D-0562; PI: Dalessandro). The $2k \times 4k$ pixels MIT Red- optimized CCD mosaic in the standard resolution mode ($\sim 0\farcs25$ pixel^{-1}) was adopted for these observations in order to sample the largest possible field of view (FOV; $\sim 6\farcm8 \times 6\farcm8$). Three pointings complementary to the ACS sample have been set up (see Figure 1) starting from $r \sim 150''$ (and reaching $r \sim 750''$) from the center of the cluster. For each pointing, eight images in the $I_{\rm BESSEL}$ band with an exposure time of $t_{\rm exp} = 240$ s each and four in $V_{\rm HIGH}$ with $t_{\rm exp} = 510$ s, have been obtained. A dither pattern of a few arcseconds has been adopted to allow for a better reconstruction of the point-spread function (PSF) and to avoid CCD blemishes and artifacts. Master bias and flat-fields have been obtained by using a large number of calibration frames. Scientific images have been corrected for bias and flat-field by using standard procedures and tasks contained in the Image Reduction and Analysis Facility.[6] The photometric analysis has been performed independently for each image and chip (see, for example, Dalessandro et al. 2014) by using DAOPHOTII (Stetson 1987). For each frame, we selected several tens of bright, not saturated, and relatively isolated stars to model the PSF, which turned out to be well reproduced by a

[6] Astronomy Observatory, which is operated by the Association of Universities for Research in Astronomy, Inc., under a cooperative agreement with the National Science Foundation.

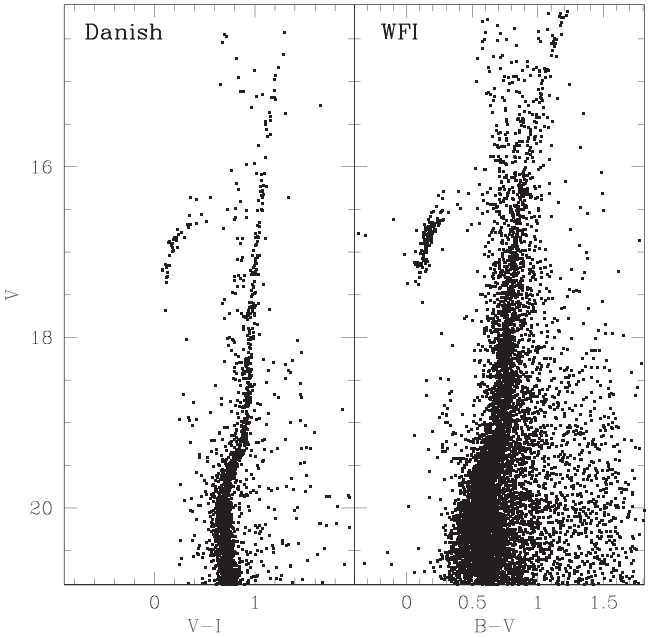

Figure 3. Left panel: $(V, V-I)$ CMD of the Danish data set published by Marconi et al. (2001). Here only the stars lying outside of the ACS FOV are shown. Right panel: $(V, B-V)$ CMD obtained from the WFI sample. In order to minimize the contamination from Galactic field stars, we show here only stars located at $r < 500''$ from the cluster center.

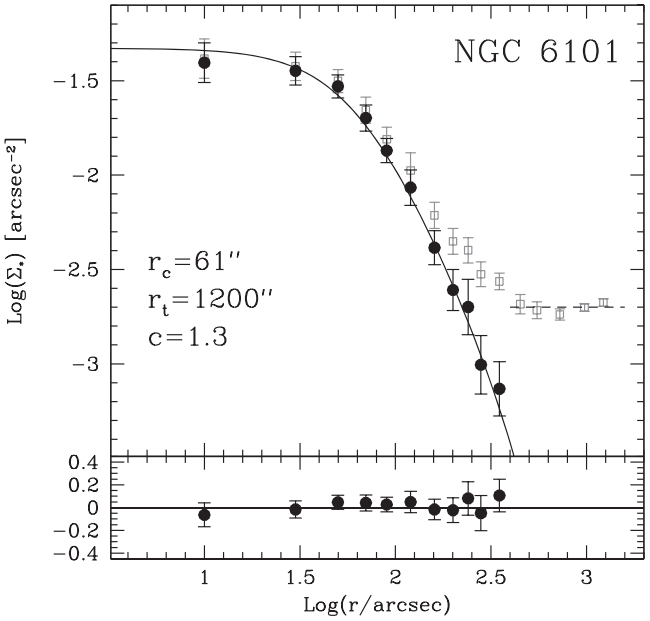

Figure 4. Observed star count density profile as a function of radius (open squares). The dashed line represents the density value of the Galactic field background, obtained averaging the five outermost points. The black filled dots are densities obtained after background subtraction (Secion 3). The best-fit single-mass King model is also overplotted to the observations (solid line). The structural parameters are labeled. The lower panel shows the residuals between the observations and the best-fit model.

Moffat function (Moffat 1969). The parameters (σ, β) describing the PSF model have been allowed to vary with a third order polynomial as a function of the instrumental coordinates (x, y) within the frame. For each chip, the best PSF model was then applied to all sources at 2σ above the background by using DAOPHOTII/ALLSTAR. We then created a master list of stars composed by sources detected in at least four frames. In the single frames, at the corresponding positions of the stars present in the master list, a fit was forced with DAOPHOTII/ALLFRAME (Stetson et al. 1994). For each star, different magnitude estimates in each filter were homogenized and their weighted mean and standard deviation were finally adopted as star magnitude and photometric error (see for example Ferraro et al. 1991, 1992). We used the stars in common with the Stetson photometric secondary standard catalog (Stetson 2000) to report the instrumental magnitudes to the V and I Johnson bands. Instrumental coordinates (x, y) have been reported to the absolute (α, δ) system by using the stars in common with the GSC2.3 catalog and the cross-correlation tool CataXcorr.[7] At this stage, the catalogs obtained for each chip are on the same photometric and astrometric system. They have been combined to form a single catalog that we defined as the FORS2 sample. Stars in common between different pointings have been used to check for the presence of residuals in the calibration procedure.

Both the FORS2 and the ACS catalogs have been corrected for differential reddening using the approach described by Milone et al. (2012). We refer the reader to this paper for details on the procedure. For each star, we used the 50 closest neighbors to compute the corresponding average differential color excess $\delta[E(B-V)]$. We adopted extinction coefficients from Cardelli et al. (1989). Over the FOV covered by the three pointings, the total variation of $E(B-V)$ amounts to only 0.06 mag. The resulting $(V, V-I)$ CMDs are shown in Figure 2.

Since the FORS2 data set saturates at $V \sim 18$ and does not provide a complete area coverage (see Figure 1), we complemented it with images obtained with the Wide Field Imager (WFI) mounted at the MPG/ESO 2.2 m telescope to homogeneously analyze the density profile of NGC 6101 (Section 3). We used six long exposure images: three in the $B_{\rm NEW}$ band with $t_{\rm exp} = 120$ s (Prop ID: 069.D-0582, PI: Ortolani) and three in $V/89_{\rm ESO843}$ with $t_{\rm exp} = 60$ s (Prop ID: 068.D-0265, PI: Ortolani). Both the pre-reduction and the photometric analysis have been performed as described above for the FORS2 data set. Also, the instrumental magnitudes have been reported to the Johnson system by using the stars in common with the catalog by Stetson (2000). A color equation was adopted to calibrate the $B_{\rm NEW}$ band, while a zeropoint was enough for the $V/89_{\rm ESO843}$ band. Instrumental coordinates have been reported to the absolute system for each of the eight WFI chips using the stars in common with GSC2.3, as done before. The resulting $(V, B-V)$ CMD is shown in the right panel of Figure 3.

We emphasize that for all catalogs, the magnitudes are in the Johnson–Cousin photometric system. To avoid confusion, in the following, we will refer to them as "B," "V," and "I."

3. DENSITY PROFILE AND CLUSTER PARAMETERS

We used the ACS and WFI data sets to compute the density profile of NGC 6101 from direct star counts. In particular, the sample is composed of all stars in the ACS catalog and those in the complementary WFI data set. We used stars with $13.5 \leqslant V \leqslant 19.5$ to avoid incompleteness and saturation problems. As

[7] CataXcorr is a code aimed at cross-correlating catalogs and finding solutions, developed by P. Montegriffo at INAF—Osservatorio Astronomico di Bologna, and successfully used by our group for the past 10 years.

done in other works (see, for example, Dalessandro et al. 2013b), we divided the FOV in 16 concentric annuli (five of them are in the ACS FOV) centered on the center of gravity ($C_{\rm grav}$), which we have adopted to be the one reported by Goldsbury et al. (2010; R.A. $=16^{\rm h}:25^{\rm m}:48\overset{\rm s}{.}12$, decl. $=-72°:12':07\overset{''}{.}9$). Each annulus has been split into an adequate number of sub-sectors (ranging from two to four) according to the local density of stars and the angular coverage in the WFI FOV. Number counts have been calculated in each subsector and the corresponding densities were obtained by dividing them by the sampled area. Particular attention has been paid to incomplete area coverage of the WFI data set starting from $r\sim 1000''$ and to the inter-chip gaps. The stellar density of each annulus was then defined as the average of the subsector densities, and its standard deviation was computed from the variance among the subsectors. We made sure to guarantee some radial overlap between the two samples in order to homogenize the two portions of the density profile. The resulting surface density profile is shown in Figure 4. We estimated the contribution of the Galactic field background by averaging the densities of the five outermost measures, corresponding to $r>400''$. We obtain an average background density of $\log(\rho_{\rm bck})\sim -2.7$ stars arcsec^{-2}. We have verified that the observed background density is fully consistent with that obtained by using the Besancon Galaxy model simulation (Robin et al. 2003) covering an area of $1°\times 1°$ centered on the position of NGC 6101 and for stars in the same magnitude limit used to build the density profile. This density has been subtracted to the observed density profile to obtain a "decontaminated" density distribution (solid symbols in Figure 4). As is apparent from the figure, the background in the external regions of NGC 6101 is not constant, which is at odds with what is expected, but it mildly increases as a function of the distance. This behavior introduces some uncertainties on the background density estimate. However, we have checked that variations of the background density within intervals compatible with the observations do not significantly affect the density distribution.

We fit the radial density profile by using an isotropic single-mass King model (King 1966), following the procedure fully described in Miocchi et al. (2013). The model best-fitting the observed density profile has a concentration of $c=1.3^{+0.15}_{-0.16}$ and a core radius of $r_c=61\overset{''}{.}3^{+6.9}_{-5.4}$, which yield a tidal radius of $r_t=1200''^{+390}_{-250}$. We also derive the projected half-light radius (effective radius) $r_h=128\overset{''}{.}2^{+16}_{-7.6}$. The newly determined structural parameters are in partial disagreement with those found in the literature and they make NGC 6101 more concentrated and extended than previously thought. In particular, r_c is compatible within the errors with the one listed by Harris (1996$r_c=58\overset{''}{.}5$), while the values of c (and as a consequence r_t) and r_h are much larger than in Harris (1996; $c=0.80$ and $r_h=63''$). The same result is also derived from the comparison with the values obtained by McLaughlin & van der Marel (2005), who quote $c=0.60$, $r_c=59\overset{''}{.}2$, and $r_h=63\overset{''}{.}6$. We argue that the difference between our parameters and the literature is mainly due to the fact that both Harris (1996) and McLaughlin & van der Marel (2005) made use of non-homogeneous surface brightness profiles that are limited to the innermost $\sim 100''$ from the center not allowing for an appropriate background subtraction.

We have estimated the distance modulus and reddening of NGC 6101 by comparing its CMD to that of M30 (NGC 7099).

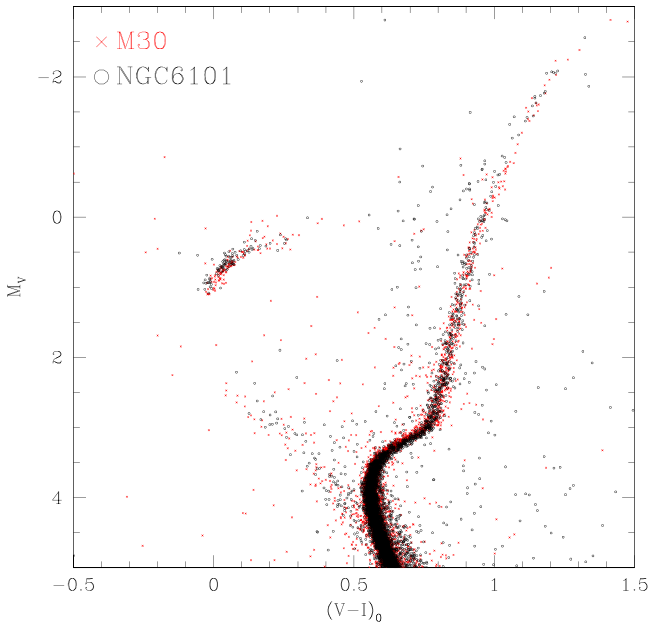

Figure 5. Superposition of the CMD of NGC 6101 (black open circles) to that of M30 (red crosses) in the absolute M_V, $(V-I)_0$ plane. For M30, we adopted the values of distance and extinction obtained by Ferraro et al. (2009). A distance modulus $(m-M)_V=16.20\pm 0.1$ and a color excess $E(B-V)=0.12$ were then adopted for NGC 6101 to match the main evolutionary sequences of M30.

M30 can be used as a template for this analysis since it has a similar metallicity ([Fe/H] $=-2.33\pm 0.2$; Carretta et al. 2009) and its distance has been robustly determined because of its proximity. To guarantee homogeneity, we compared the ACS sample of NGC 6101 with the CMD of M30 obtained with the same instrument within the same survey (Sarajedini et al. 2007).

We reported the CMD of M30 in the absolute plane M_V, $(V-I)_0$ by adopting a distance modulus of $(m-M)_V=14.80$ and a reddening of $E(B-V)=0.03$ (Ferraro et al. 2009). To overlap the CMDs and align all of the main evolutionary sequences in the absolute plane (see Figure 5), we needed to adopt $(m-M)_V=16.20\pm 0.10$ and a reddening of $E(B-V)=0.12\pm 0.02$ for NGC 6101, which yield to a true (unreddened) distance modulus $(m-M)_0=15.83\pm 0.12$ and thus to a distance $d=14.6\pm 0.8$ Kpc. We use these values throughout the paper.

These values are slightly larger than those obtained in the literature, but in most cases they are still compatible within the errors. In particular, Harris (1996) report $(m-M)_V=16.07\pm 0.1$ and $E(B-V)=0.05$, Sarajedini & Da Costa (1991) found $(m-M)_V=16.12\pm 0.1$ and $E(B-V)=0.06$, M01 obtained $(m-M)_V=16.12\pm 0.03$ $E(B-V)=0.1$, while Cohen et al. (2011) estimated $(m-M)_V=16.00\pm 0.03$ $E(B-V)=0.1$ from the average luminosity of RR Lyrae stars and zero-age horizontal branch fit.

4. THE BSS RADIAL DISTRIBUTION

BSSs in GCs are commonly defined as those stars located along an extrapolation of the MS, in a region brighter and bluer than the turn-off (TO) point in the optical CMD (Sandage 1962). Their location suggests that they are more massive than the current cluster population (see, for example, Ferraro et al. 2006a; Lanzoni et al. 2007a). Indeed, observational evidence

(Shara et al. 1997; Gilliland et al. 1998; Fiorentino et al. 2014) showed that BSSs have masses of $M \sim 1.2$–$2.0\,M_{\odot}$ compared to a mass of $\sim 0.8\,M_{\odot}$ for stars at the MS–TO of an old stellar system.

Because of their mass, BSSs are heavily affected by dynamical friction and thus they can be used as natural test particles to probe the internal dynamics of stellar aggregates. In particular, their radial distribution has been found to probe the efficiency of dynamical friction (Mapelli et al. 2006; Alessandrini et al. 2014; Miocchi et al. 2015). Ferraro et al. (2012) suggested that the BSS radial distribution can be used to define the so called *dynamical clock*, which is a powerful indicator of the cluster dynamical age. In this picture, GCs with a flat BSS radial distribution are dynamically young stellar systems and they are defined as *Family I* GCs, clusters with a bimodal radial distribution have intermediate dynamical ages (*Family II*), while those with a centrally peaked and monotonically decreasing BSS distribution are dynamically old (*Family III*).

The BSS population of NGC 6101 has been studied by Sarajedini & Da Costa (1991) and M01. In particular, M01 also studied the BSS radial distribution by using a combination of *HST* Wide Field Planetary Camera 2 (defined *"hst" sample*) and ground-based data (*"ground" sample*) corresponding to the Danish sample defined in Section 2. By using cumulative radial distributions and Kolmogorov–Smirnov tests, they concluded that BSSs have a large probability (84%) to have been extracted from the same parent population as HB, while HB and Tip red giant branch (RGB) stars being more centrally concentrated than MS–TO stars. They interpreted these results as evidence of mass segregation.

4.1. Population Selections

We studied the BSS population of NGC 6101 by using the ACS and Danish data sets. In detail, the final sample consists of stars in the ACS catalog and those present in the Danish data set and complementary to the ACS FOV (see Figure 1). In this way, the central region of NGC 6101 is homogeneously covered up to a distance of $r \sim 250''$ (corresponding to about $4 \times r_c$) from $C_{\rm grav}$. While the WFI data set covers a larger FOV and ensures a complete sampling of the cluster up to r_t, we preferred this combination of catalogs for the BSS analysis because of the better photometric quality of the data (see Figures 2 and 3).

As done in previous works (see, for example, Ferraro et al. 1997, 2004; Lanzoni et al. 2007a, 2007b; Dalessandro et al. 2008a and reference therein), in order to study the BSS radial distribution, we need a homogeneous selection of BSSs and at least one reference stellar population. For the case of NGC 6101 we selected HB, RGB, and MS–TO stars as references.

BSSs have been selected following the definition of stars bluer and brighter than TO. The selection box shown in Figure 6 follows the well defined BSS sequence brighter than $V = 20$. An additional constraint on the color ($(V - I) < 0.5$) has been adopted to avoid contamination and blends from MS and SGB stars. In this way, we selected 52 BSSs, 33 in the ACS FOV, and 19 in the complementary Danish sample. Because of the more conservative selection criteria adopted in this work, the BSS sample is smaller than the one obtained by M01, who identified 73 BSSs adopting different magnitude and color selections. As for the reference populations, we

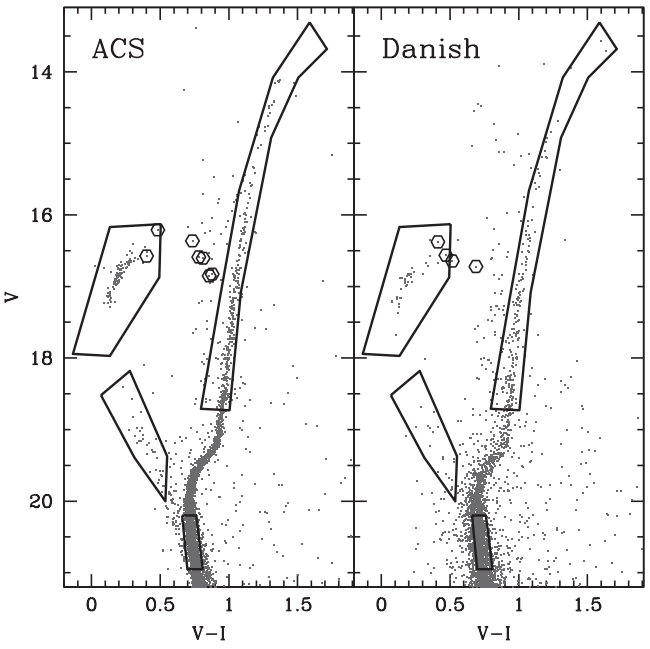

Figure 6. Zoomed view of the (V, $V - I$) ACS and ground-based CMDs. Selection boxes for MS, RGB, HB, and BSSs stars are shown. The RR Lyrae identified in the HB sample are marked with open hexagons.

selected RGB stars along the RGB, for which $13.5 < V < 18.7$. With these limits we selected a total of 510 RGB stars, 328 in the ACS sample and 182 in the Danish one. We selected HB stars following their well defined sequence for $(V - I) < 0.5$ to minimize the impact of field contamination. In fact, as is apparent from Figure 6, the Galactic field describes a vertical sequence in the color range of $0.7 < (V - I) < 0.9$. The HB selection box is shown in Figure 6 and encloses 137 stars. By using the list of known RR lyrae stars (Liller 1981; Cohen et al. 2011; Fitzgerald et al. 2012), we identified 11 stars in common, 7 in the ACS and 4 in the Danish FOVs. The RR Lyrae falling outside the HB selection were added to the HB sample. In this way, we count 102 and 42 HB stars in the ACS and Danish samples respectively. In order to provide a direct comparison with M01, we also used MS–TO stars as additional reference populations. They have been selected approximately within the limits of $0.65 < (V - I) < 0.80$ and $20.2 < V < 20.9$. It is worth noting that in this magnitude range, MS stars have a completeness of 100% both in the ACS (see Section 5.1) and in the complementary data set (M01). We count 3125 MS–TO stars in total, 2375 in the ACS and 750 in the complementary Danish FOVs.

We obtained an estimate of the Galaxy field contamination by using the Besancon Galaxy model simulation (see Section 3). We counted the number of stars lying in the adopted (V, $V - I$) selection boxes. We find 125 and 455 Galactic field MS–TO and RGB stars, respectively, yielding densities of $\rho_{\rm bck}^{\rm MS} \sim 1 \times 10^{-4}$ stars arcsec^{-2} and $\rho_{\rm bck}^{\rm RGB} \sim 3.5 \times 10^{-4}$ stars arcsec^{-2}. We do not find any field star falling in the boxes adopted to select HB and BSS stars.

4.2. Radial Distributions

We first compared the BSS cumulative radial distribution to those of the reference populations. As done in Dalessandro et al. (2013a), we took into account the effect of Galactic field contamination by statistically decontaminating the RGB and

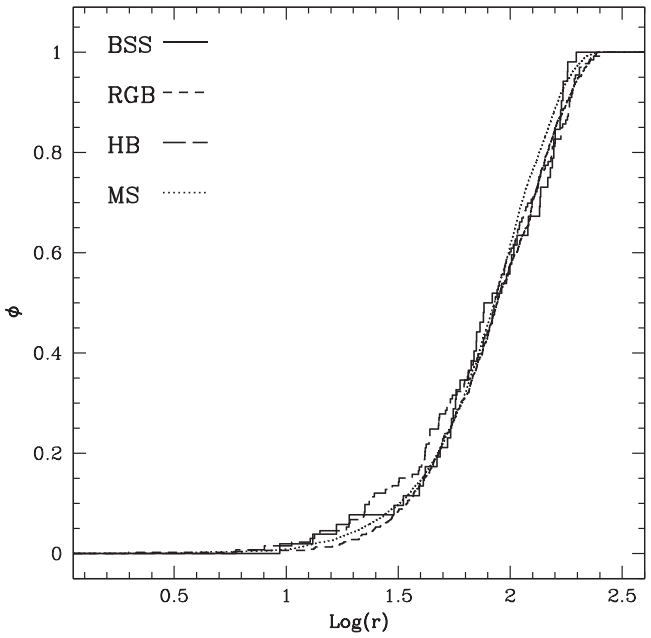

Figure 7. Cumulative radial distribution of the statistically decontaminated populations.

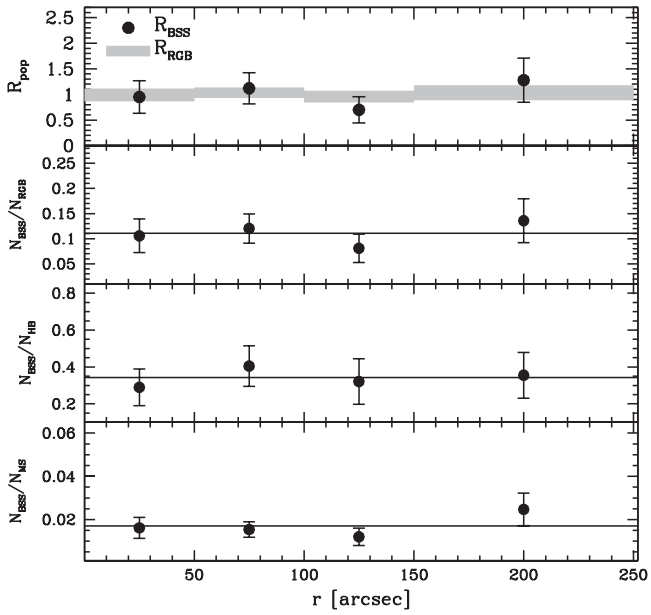

Figure 8. From top to bottom, radial distributions of the double normalized ratios of the BSS ($R_{\rm BSS}$; solid circles) and RGB stars ($R_{\rm RGB}$; gray regions), and the specific frequencies $N_{\rm BSS}/N_{\rm RGB}$, $N_{\rm BSS}/N_{\rm HB}$, and $N_{\rm BSS}/N_{\rm MS}$ (solid circles).

MS populations. We divided the FOV into four concentric annuli centered on $C_{\rm grav}$ and, for each of them, we randomly subtracted a number of stars corresponding to the average field densities quoted above. The decontaminated cumulative radial distributions are shown in Figure 7. As is apparent, the four populations show very similar behaviors. Indeed, when a KS test is applied, we obtain probabilities of $P_{\rm BSS/RGB} \sim 18\%$, $P_{\rm BSS/HB} \sim 20\%$ and $P_{\rm BSS/MS} \sim 65\%$ that they are extracted from a different parent population. Since they are well below the canonical probability limit of 95%, we can conclude that in all cases the differences in the observed radial distributions are not significant. Also, we obtain that the radial distributions of the parent populations (HB, RGB, and MS) are consistent with all being extracted from the same parent distribution. These results are in good agreement with what was found by M01 so long as the analysis is limited to HB, RGB, and BSS stars, while a different behavior is observed for MS stars. In fact, M01 found the BSS population to be significantly more centrally segregated than MS stars. In order to more accurately compare our results with M01, we also used their *"hst" sample* and selected stellar populations using the same boxes defined above. Also in this case, we do not find any significant difference among the radial distribution of RGB, HB, and BSS and that of MS stars.

We also analyzed the radial distribution of the specific frequencies $N_{\rm BSS}/N_{\rm RGB}$, $N_{\rm BSS}/N_{\rm HB}$, and $N_{\rm BSS}/N_{\rm MS}$, where $N_{\rm POP}$ is the number of stars in the corresponding population. We divided the FOV into four concentric annuli centered on $C_{\rm grav}$ and, in each of them, we counted the number of BSS and that of the reference population stars. Galaxy field contamination has been accounted for as described above. The radial distributions of the specific frequencies are shown in Figure 8. In all cases, and in agreement with what was observed from the cumulative radial distributions, we find that these ratios are almost constant over the entire extension of the ACS + Danish FOV ($r < 250''$).

We also computed the double normalized ratio ($R_{\rm POP}$[8]; Ferraro et al. 1993) for BSS and RGB stars. In particular, for the same annuli used before, we estimated the sampled luminosity using the best-fit King model discussed in Section 3, a distance modulus $(m - M)_V = 16.20 \pm 0.1$ and reddening $E(B - V) = 0.12$. We find that the $R_{\rm POP}$ is constant for both RGB stars and BSSs as expected for any post-MS population (Renzini & Fusi Pecci 1988). The same result is obtained when HB and MS stars are considered.

Although this analysis does not cover the entire extension of NGC 6101 (it is limited to $\sim 2r_h$), we note that the considered data sets sample about 70% of the total luminosity of the cluster. On the basis of what was observed in tens of GCs (Ferraro et al. 2012), we do not expect any significant deviation from the general behavior at larger distances. Therefore, we can safely conclude that the BSS radial distribution of NGC 6101 is flat (i.e., indistinguishable from that of the reference populations). Such a distribution is not common for GCs and it has been observed only in few other cases so far (ω Centauri—Ferraro et al. 2006a; NGC 2419—Dalessandro et al. 2008b; Palomar 14—Beccari et al. 2011; Ter 8 and Arp 2—Salinas et al. 2012). As for those GCs, a flat BSS radial distribution is a strong indication of the absence of mass segregation in NGC 6101.

5. THE BINARY FRACTION RADIAL DISTRIBUTION

The fraction of binaries is an essential component of the formation and evolutionary processes of stellar systems. In dynamically active aggregates, such as GCs, binaries are thought to promote the formation of exotic objects like BSSs, X-ray sources, and Millisecond Pulsars (see, e.g., Mc Crea et al. 1964, Paresce et al. 1992; Heinke et al. 2003; Ferraro et al. 2006b, 2009; Pooley & Hut 2006; Xin et al. 2015).

[8] $R_{\rm POP} = (N_{\rm POP}/N^{\rm tot}_{\rm POP})/(L^{\rm samp}/L^{\rm samp}_{\rm tot})$, where POP=RGB and BSS. $L^{\rm samp}$ is the luminosity sampled in each annulus and estimated by using the best-fit King model, distance modulus, and reddening derived in Section 3. $L^{\rm samp}_{\rm tot}$ is instead the luminosity sampled in the entire field of view.

Binaries are typically more massive than the average single star mass in GCs ($\langle m \rangle \sim 0.3\,M_{\odot}$), therefore, they tend to sink toward the center of GCs because of dynamical friction. As a consequence, their radial distribution can also be a useful tool to constrain the dynamical state of GCs.

Up to now, three main techniques have been used to measure the binary fraction: (1) radial velocity variability (e.g., Mathieu & Geller 2009), (2) the search for eclipsing binaries (e.g., Cote et al. 1996; Mateo 1996), and (3) studies of the distribution of stars along the cluster MS in CMDs (Romani & Weinberg 1991; Bellazzini et al. 2002). In this paper, we used the latter approach by following the method described by Bellazzini et al. (2002; see also Sollima et al. 2007; Dalessandro et al. 2011; Beccari et al. 2013). The basic idea is that the magnitude of the binary system corresponds to the luminosity of the primary star (more massive) increased by that of the companion. Stars on the MS obey a mass–luminosity relation, hence the luminosity of the binary system is a function of the mass ratio $q = m_2/m_1$ of the two components (where m_1 and m_2 are the masses of the primary and secondary, respectively). Since q can assume any value between 0 and 1, in CMDs, binaries describe a "secondary MS" in the CMD, i.e., they generate a broadening of the single star's MS, toward higher luminosities.

The binary fraction (ξ) of the central regions of NGC 6101 has been estimated by Sollima et al. (2007) and Milone et al. (2012). In this work, we recomputed the central binary fraction by using the ACS sample for homogeneity, and we extended the analysis to the cluster peripheries by using the FORS2 data set.

5.1. Artificial Stars Experiment and Galaxy Contamination

In order to estimate the binary fraction by analyzing the "secondary MS," a number of spurious effects should be considered. First, the Galactic field contamination should be properly taken into account. Then, robust measures of source of broadening, like blending and photometric errors, should be considered. These factors are related to the quality of the data and can be properly studied through artificial star experiments.

For the ACS sample, we used the artificial star catalog provided with the real star catalog and available at the "ACS Survey of Galactic Globular Clusters" web page.[9] For the FORS2 sample, we performed a large number of artificial star experiments. We followed the method described by Bellazzini et al. (2002; see also Dalessandro et al. 2011). We generated a catalog of simulated stars with an I-band input magnitude ($I_{\rm in}$) magnitude extracted from an LF modeled to reproduce the observed LF in that band and extrapolated beyond the limiting magnitude. Then, to each star extracted from the LF, we assigned a $V_{\rm in}$ magnitude by means of an interpolation along the mean ridge line of the cluster.

Artificial stars were added to real images by using the DAOPHOTII/ADDSTAR software. In order to avoid "artificial crowding," stars were placed into the images following a regular grid composed by 35 × 35 pixel cells (corresponding approximately to eight to nine times the usual FWHM of stars for these images) in which only one artificial star for each run was allowed to lie. More than 250,000 stars have been simulated for the entire FOV covered by the FORS2 sample. The photometric reduction process used for the artificial star experiments is exactly the same as described in Section 2. Those stars recovered after the photometric analysis also have values of $V_{\rm out}$ and $I_{\rm out}$. As already noticed in Dalessandro et al. (2011; see also Milone et al. 2012), the MSs of the artificial star CMDs are narrower than the observed ones. One possible reason for this effect, is that the formal photometric errors of the artificial-star catalogs systematically underestimate the true observational uncertanties. Another possibility is that the broadening of the observed data is due to some physical effects, such as the presence of multiple populations along the MS. Irrespective of the origin and as done in Dalessandro et al. (2011), we increased the formal artificial-star catalog errors in order to reproduce the observed error distribution as a function of magnitude. The curves of photometric completeness (C), defined as the ratio between the number of stars recovered at the end of the procedure and the total number of stars actually simulated, are shown in Figure 9 for different radial bins.

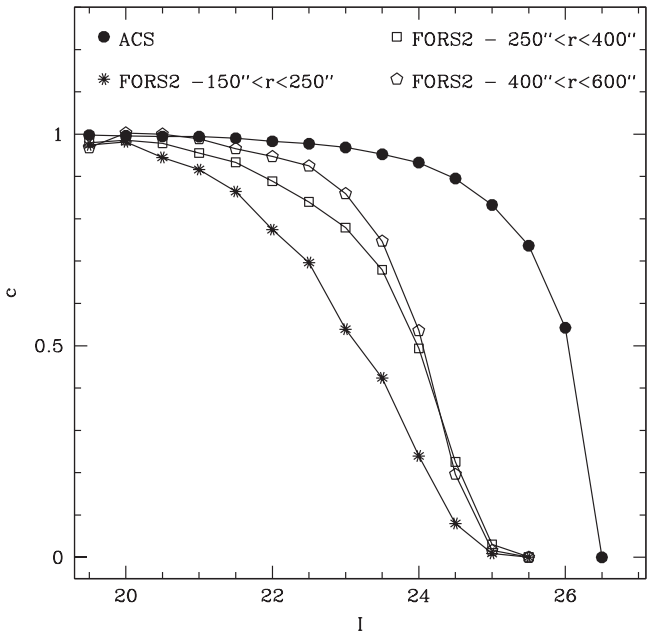

Figure 9. Photometric completeness C as a function of the I band magnitude for the ACS and the FORS2 data sets and for different radial bins.

For a proper measurement of the binary fraction, we performed a detailed study of the field contamination, using the same Besancon Galaxy model catalog described in Section 4.

5.2. The Binary Fractions

The high photometric quality and the spatial coverage provided by the combination of the ACS and FORS2 data sets, allow us to study the binary fraction radial distribution from the core up to 600″ from the cluster center.[10] We divided the FOV in four concentric annuli roughly corresponding to 0.0–1.0 r_h, 1.0–2.0 r_h, 2.0–3.5 r_h, and 3.5–5 r_h, and we estimated both the minimum ($\xi_{\rm min}$) and the global binary fractions ($\xi_{\rm TOT}$) following the approach described by Bellazzini et al. (2002). The analysis was performed for stars with $19 \leqslant I \leqslant 22$, where

[9] http://www.astro.ufl.edu/~ata/public_hstgc/

[10] While the FORS2 data set extends out to $r \sim 800''$, we preferred to limit the analysis at $r \sim 600''$ where the fraction of covered area coverage is more complete and the number of detected stars is appropriate for an accurate analysis of the binary population.

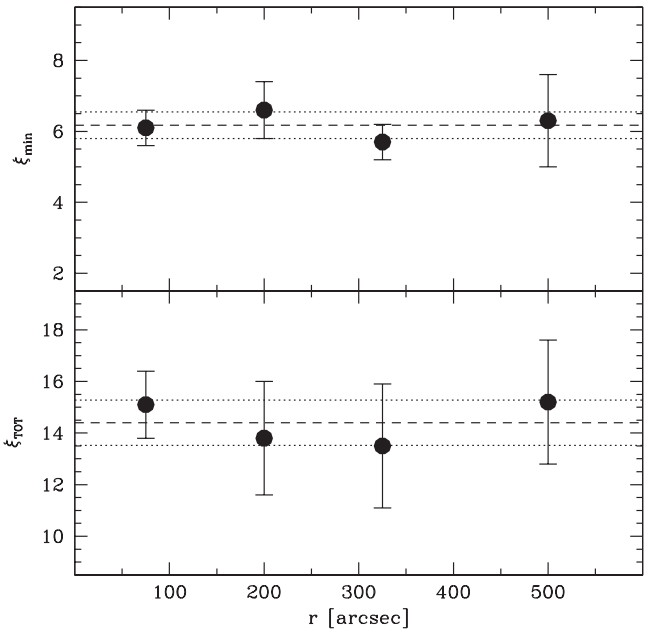

Figure 10. Minimum and global binary fractions as a function of the radial distance from the cluster center. The dashed lines represent the mean value, while the dotted ones define the 1σ level.

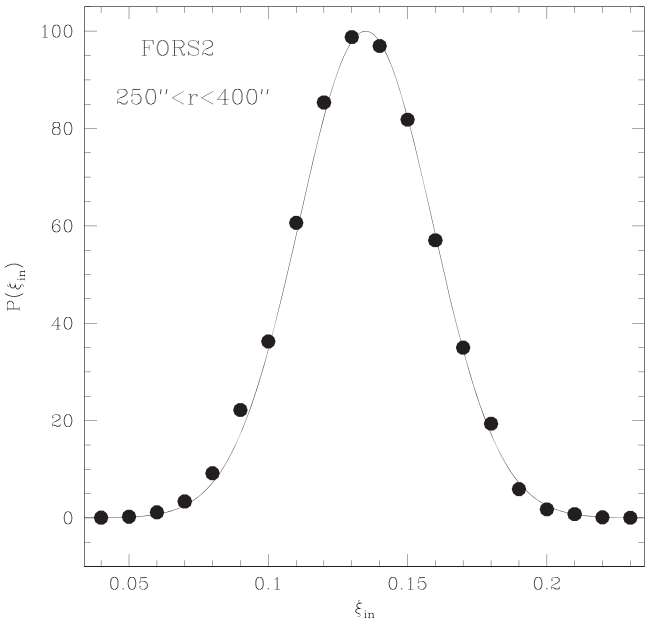

Figure 11. Probability distribution of the adopted input binary fraction ξ_{in}, for the case of the FORS2 sample and for $250'' < r < 400''$.

the completeness parameter (C) is safely larger than 50%. This interval corresponds to a mass range of $0.55 < m/M_{\odot} < 0.80$ for a single star along the MS, according to an isochrone of 12 Gyr and $Z = 0.003$ (Bressan et al. 2012).

First, we measured $\xi_{\rm min}$, which is the fraction of binaries with a mass ratio $q_{\rm min}$ large enough to make them clearly distinguishable from single MS stars. The value of $q_{\rm min}$ depends on the photometric errors: we considered a color range equal to three times the photometric error from the MS ridge line (see Figure 3 in Dalessandro et al. 2011); in the considered magnitude interval, and for the entire sample, such a color difference corresponds to $q_{\rm min} \sim 0.4$. The contamination from blended sources and non-member stars has been accounted for by means of the artificial star catalogs and the Besancon model simulation (Section 5.1). The radial distribution of $\xi_{\rm min}$ is shown in Figure 10. As already observed for BSSs, binaries show no significant evidence of mass segregation. In fact, their radial distribution is almost flat around a mean value $\xi_{\rm min} = (6.2 \pm 0.4)\%$. Such a value is slightly larger than what was obtained by Milone et al. (2012) only in the central regions ($q_{\rm min} = 4.8 \pm 0.3\%$). It is important to note, however, that Milone et al. (2012) considered only binaries with a mass ratios larger than ours ($q > 0.5$).

As a second step to the analysis, we also estimated $\xi_{\rm TOT}$. To this aim, we created hundreds of synthetic CMDs including single and binary stars for different input values of the global binary fraction ($\xi_{\rm IN}$), for each run. To simulate the binaries, we randomly extracted $N_{\rm bin}$ values of the mass of the primary from Kroupa (2002) initial MF and $N_{\rm bin}$ values of the mass of the primary component from the Fisher et al. (2005) mass ratio distribution, $f(q)$, which is one of the unknowns in this kind of analysis. The impact of adopting different mass ratio distributions has been discussed in Sollima et al. (2007) and Dalessandro et al. (2011). To generate the sample of single MS stars we adopted the best fit to the observed MF, which is discussed in detail in Section 6. In Dalessandro et al. (2011), we have verified that the adoption of different present day MFs to simulate MS stars has a negligible impact on the final result. $\xi_{\rm TOT}$ was then determined from the comparison between the artificial and the observed CMDs: the value of $\xi_{\rm IN}$ providing the best match between the two CMDs is adopted as a global binary fraction $\xi_{\rm TOT}$. In particular, from the simulated catalog, we computed the ratio $r_{\rm sim} = N_{\rm bin}^{\rm sim}/N_{\rm MS}^{\rm sim}$ between the number of binary stars defined as before and that of the synthetic MS population. The same was done for the observed CMD, thus obtaining $r_{\rm sim} = N_{\rm bin}^{\rm obs}/N_{\rm MS}^{\rm obs}$. For different values of $\xi_{\rm IN}$, we computed the penalty function $\chi^2(\xi_{\rm IN})$ defined as the summation of $(r_{\rm sim} - r_{\rm obs})^2$ and the relative probability $P(\chi^2)$ was derived (Figure 11). The mean of the best-fitting Gaussian is adopted as well as the best-fit value of the global binary fraction $\xi_{\rm TOT}$. The radial distribution of $\xi_{\rm TOT}$ is shown in Figure 10. Similar to the minimum binary fraction, $\xi_{\rm TOT}$ shows no variation as a function of the distance from the center in the FOV covered in this analysis. This results confirms that NGC 6101 has not experienced complete relaxation yet and does not show any evidence of mass segregation among its populations.

The mean value of the global binary fraction is $\xi_{\rm TOT} = (14.4 \pm 0.9)\%$. This value is in good agreement with the one obtained by Sollima et al. (2007) in the ACS FOV ($\xi_{\rm TOT} = 15.6 \pm 1.3\%$), while it is significantly larger than the one estimated by Milone et al. (2012; $\xi_{\rm TOT} = 9.6 \pm 0.6\%$). Note, however, that Milone et al. (2012) determined the value of $\xi_{\rm TOT}$ assuming that it is twice the value of $\xi_{\rm min}$.

6. LUMINOSITY AND MASS FUNCTION RADIAL VARIATIONS

To further investigate the mass segregation phenomenon in NGC 6101, we analyzed the radial variation of the LF of MS stars. LFs give information about the effect of cluster internal dynamics on stars in a wide range of masses, including the faint-end of the MS where most of the cluster mass lies. In relaxed stellar systems, the slope of the LFs is expected to vary as a function of the distance from the cluster center, with

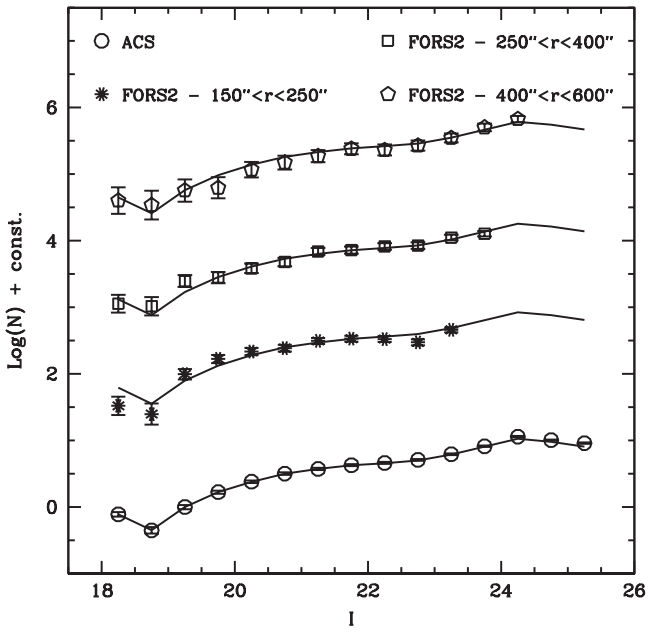

Figure 12. LFs in the I band obtained from the ACS and the FORS2 data sets in different radial bins. Measurements are shifted by an arbitrary amount to make the plot more readable. The solid line is the LF obtained in the ACS sample for $r < r_h$. It has been overplotted to the outer LFs for comparison.

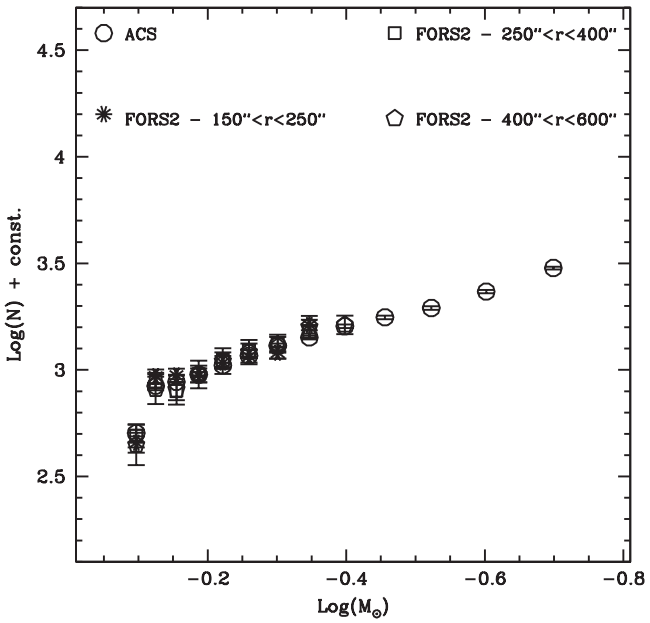

Figure 13. MFs derived by using the Baraffe et al. (1997) mass–luminosity relation. Radial bins and symbols are the same as in Figure 12.

indexes decreasing as the distance increases, because of the differential effect of mass segregation.

To study the LF of NGC 6101, we used the ACS and FORS2 samples. We selected a sample of bona fide stars along the MS, defined as those stars located within 3σ from the mean ridge line, where σ is the combined photometric uncertainty in the V and I bands. We used the same radial bins defined in Section 5 for the binary fraction analysis. For each radial interval, we obtained the completeness-corrected LF for stars fainter than $V = 18$ and reaching the magnitude limit where the completeness parameter C is 50%. Completeness has been derived by means of the artificial star catalog described in Section 5.1 (see Figure 9). The LFs obtained in the four radial bins are shown in Figure 12. We took the LF corresponding to the innermost radial bin as reference for comparison with the LFs in the other radial ranges. The line connecting the points of the reference LF is plotted as a solid line in Figure 12. As is apparent, it well reproduces the behavior observed in the more external radial bins after a proper normalization. The key result of Figure 12 is that, in the range of magnitude and radial extension ($0 < r < 5r_h$) covered by our analysis, the shape of the different LF is clearly the same and any subtle difference lies well within the combined uncertainty of the LFs and of the adopted normalization.

We derived the MF of the same bona fide stars used for the LF and within the same magnitude limits. Masses have been obtained by using the Baraffe et al. (1997) mass–luminosity relation. The MFs obtained in the same radial bins as the LFs are shown in Figure 13. The MF obtained in the ACS sample goes down to $m \sim 0.15\,M_\odot$, while it reaches at most $m \sim 0.35\,M_\odot$ in the FORS2 data set. As done before, we used the MF of the innermost radial bin as reference, and we normalized the more external ones to this by using number counts in the mass range $(0.5 < m/M_\odot < 0.7)$. As is apparent from Figure 13, and in agreement with what was obtained from the analysis of the LFs, all MFs are virtually indistinguishable.

7. DISCUSSION

Three distinct indicators, namely the radial distribution of BSSs, binary stars, and the LF of MS stars have been investigated to study the mass segregation in NGC 6101. We have traced this effect by using stars in a wide range of masses, going from $\sim 0.35\,M_\odot$, corresponding to the lowest mass MS stars, up to $\sim 1.4\,M_\odot$ reached by the highest mass BSSs and binaries. The results clearly indicate that the clusters do not show evidence of mass segregation up to $r \sim 600''$ ($\sim 5r_h$) from the cluster center.

Only a few other GGCs are known to be in such a dynamical state: massive systems ($M_V < -10$), namely ω Centauri (Ferraro et al. 2006a) and NGC 2419 (Dalessandro et al. 2008b), and three GCs that are at the low-mass end of the distribution ($M_V \sim -5$), namely Palomar 14 (Beccari et al. 2011), Ter 8, and Arp 2 (Salinas et al. 2012). Similarly to these clusters, NGC 6101 can be considered dynamically young.

Starting from the new structural parameters obtained in Section 3, we derived the central ($t_{\rm rc}$) and half mass–radius ($t_{\rm rh}$) relaxation times following the formulae by Spitzer (1987). We adopted the same values of $(m - M)_V$ and $E(B - V)$ used in Section 4.2, which yield a distance from the Sun of $d = 14.6 \pm 0.8$ Kpc (see Section 3). We estimated the total cluster mass M_t by adopting an integrated V magnitude $V_t = 9.2$ (Harris 1996) and mass-to-light ratios $M/L_V = 3.17$ and 2.07 (Maraston 1998), appropriate for a Salpeter and Kroupa IMF, respectively, and for a population of metallicity [Fe/H] $= -2.25$ and age $t = 13$ Gyr. We obtained $M_t = (1.2\text{–}1.7) \times 10^5\,M_\odot$ which gives a central mass density of $\rho_{M,0} = 68.5\,M_\odot\,{\rm pc}^{-3}$. We thus obtained $t_{\rm rc} \sim 1.3$ Gyr and $t_{\rm rh} \sim 5.4\text{–}6.3$ Gyr. The value of $t_{\rm rc}$ is consistent with what was reported by Harris (1996), while $t_{\rm rh}$ is about three times larger than the Harris value ($t_{\rm rh} \sim 1.7$ Gyr) and more than five times larger than the one derived by McLaughlin & van der Marel

(2005) ($t_{\rm rh} \sim 0.9$ Gyr). This is qualitatively in agreement with r_h being larger than previous estimates reported in the literature.

We note, however, that both $t_{\rm rc}$ and $t_{\rm rh}$ are significantly less than the age of NGC 6101 ($t_{\rm age} = 13 \pm 1$ Gyr; Dotter et al. 2010). Therefore, some evidence of mass segregation should be visible, at odds with the observed flat distribution of BSS and binaries, and the constant slope of the MFs and LFs. In the cases of NGC 2419 and Palomar 14, $t_{\rm rh}$ has been estimated to be ∼20 Gyr (Dalessandro et al. 2008b; Sollima et al. 2011), in good agreement with the observational evidence of a lack of mass segregation, at least in the external regions. However, also for NGC 2419, the central relaxation time is significantly less ($t_{\rm rc} \sim 6$ Gyr) than the age of the cluster ($t = 12$ Gyr) and Ferraro et al. (2006a) found for ω Centauri a relatively short relaxation time ($t_{\rm rh} \sim 5$ Gyr), as for NGC 6101. In the case of ω Centauri a number of possibilities to understand this apparent disagreement between observations and theoretical results were examined. Cluster rotation can play a role. In fact angular momentum tends to keep stars out of the core, balancing the effect of mass segregation (Spurzem 2001). Another possibility is that ω Centauri could have been hundreds of times more massive in the past than observed today. Indeed, it has been suggested to be the relic of a partially disrupted galaxy (Bekki & Freeman 2003; Tsuchiya et al. 2004). The same argument can be applied to NGC 2419 (van den Bergh & Mackey 2004; Mackey & van den Bergh 2005) and the extended tidal tails observed around Palomar 14 (Sollima et al. 2011) would suggest that it experienced quite recent and efficient tidal stripping events.

For the case of NGC 6101, no evidence of internal rotation are known. However, we may speculate that NGC 6101 could have experienced a quite complex dynamical history. By means of dynamical simulations, Martin et al. (2004) suggested that NGC 6101 can be associated to the Canis Major dwarf galaxy accreted to the Galactic halo after an encounter between the dwarf and the dark matter halo of the Milky Way. Indeed, the kinematical properties of NGC 6101 are atypical for systems with its metallicity and age. In fact, it is one of the very few metal-poor and old GGCs with a retrograde motion (Geisler et al. 1995; Rutledge et al. 1997). Mackey & Gilmore (2004) suggested that the existence of old GCs with large cores in a relative proximity to the Galactic center (as for the case of NGC 6101) can be explained by the fact that they follow wide orbits in which they spend little time close to the Galactic center. Alternatively, they could have been accreted only recently by the Galactic halo.

In this respect, it is interesting to note that a linear fit to the MFs in Figure 12 limited to the stars with $m < 0.75\,M_{\odot}$ gives a power-law index of $\alpha \sim -0.9$. With such a value and with the new estimate of the central concentration obtained in Section 3 ($c = 1.3$), NGC 6101 would nicely fit the correlation found by De Marchi et al. (2007) according to which less concentrated GCs tend to have flatter MFs. This behavior was interpreted by the authors as an indication of a more efficient loss of low-mass stars via evaporation and tidal stripping in less concentrated clusters. To support this possibility, evidence of tidal arms and distortions should be searched for this cluster.

On one hand, the observational facts collected in the case of NGC 2419, ω Cen, and NGC 6101 suggest that the current theoretical estimates of the central relaxation time are extremely rough and must be used (at least in absolute terms) with caution. On the other hand, the nice agreement among the different mass segregation indicators used in the case of NGC 6101 provides additional support for the use of the radial distribution of BSS (the so-called "dynamical clock") as a powerful indicator of the dynamical evolution of stellar systems (Ferraro et al. 2012). In fact, among the adopted mass-segregation indicators, BSSs are significantly brighter than the others (MS stars and binaries), their analyses are simpler and less prone to observational bias (as completeness) and assumptions. Hence the BSS radial distribution represents the clearest indicator of mass segregation in stellar systems.

This research is part of the project COSMIC-LAB (http://www.cosmic-lab.eu) funded by the European Research Council (under contract ERC-2010-AdG-267675).

REFERENCES

Alessandrini, E., Lanzoni, B., Miocchi, P., Ciotti, L., & Ferraro, F. R. 2014, ApJ, 795, 169
Anderson, J., Sarajedini, A., Bedin, L. R., et al. 2008, AJ, 135, 2055
Baraffe, I., Chabrier, G., Allard, F., & Hauschildt, P. H. 1997, A&A, 327, 1054
Baumgardt, H., Côté, P., Hilker, M., et al. 2009, MNRAS, 396, 2051
Beccari, G., Dalessandro, E., Lanzoni, B., et al. 2013, ApJ, 776, 60
Beccari, G., Sollima, A., Ferraro, F. R., et al. 2011, ApJL, 737, LL3
Bekki, K., & Freeman, K. C. 2003, MNRAS, 346, L11
Bellazzini, M., Dalessandro, E., Sollima, A., & Ibata, R. 2012, MNRAS, 423, 844
Bellazzini, M., Fusi Pecci, F., Messineo, M., Monaco, L., & Rood, R. T. 2002, AJ, 123, 1509
Bressan, A., Marigo, P., Girardi, L., et al. 2012, MNRAS, 427, 127
Cardelli, J. A., Clayton, G. C., & Mathis, J. S. 1989, ApJ, 345, 245
Carretta, E., Bragaglia, A., Gratton, R., D'Orazi, V., & Lucatello, S. 2009, A&A, 508, 695
Cohen, R. E., Sarajedini, A., Kinemuchi, K., & Leiton, R. 2011, ApJ, 727, 9
Cote, P., Pryor, C., McClure, R. D., Fletcher, J. M., & Hesser, J. E. 1996, AJ, 112, 574
Dalessandro, E., Ferraro, F. R., Lanzoni, B., et al. 2013a, ApJ, 770, 45
Dalessandro, E., Ferraro, F. R., Massari, D., et al. 2013b, ApJ, 778, 135
Dalessandro, E., Lanzoni, B., Beccari, G., et al. 2011, ApJ, 743, 11
Dalessandro, E., Lanzoni, B., Ferraro, F. R., et al. 2008a, ApJ, 6677, 1069
Dalessandro, E., Lanzoni, B., Ferraro, F. R., et al. 2008b, ApJ, 681, 311
Dalessandro, E., Pallanca, C., Ferraro, F. R., et al. 2014, ApJL, 784, LL29
De Marchi, G., Paresce, F., & Pulone, L. 2007, ApJL, 656, L65
Dotter, A., Sarajedini, A., Anderson, J., et al. 2010, ApJ, 708, 698
Ferraro, F. R. 2006b, arXiv:astro-ph/0601217
Ferraro, F. R., Beccari, G., Dalessandro, E., et al. 2009, Natur, 462, 1028
Ferraro, F. R., Beccari, G., Rood, R. T., et al. 2004, ApJ, 603, 127
Ferraro, F. R., Clementini, G., Fusi Pecci, F., & Buonanno, R. 1991, MNRAS, 252, 357
Ferraro, F. R., Clementini, G., Fusi Pecci, F., Sortino, R., & Buonanno, R. 1992, MNRAS, 256, 391
Ferraro, F. R., D'Amico, N., Possenti, A., Mignani, R. P., & Paltrinieri, B. 2001, ApJ, 561, 337
Ferraro, F. R., Dalessandro, E., Mucciarelli, A., et al. 2009, Natur, 462, 483
Ferraro, F. R., Lanzoni, B., Dalessandro, E., et al. 2012, Natur, 492, 393
Ferraro, F. R., Paltrinieri, B., Fusi Pecci, F., et al. 1997, A&A, 324, 915
Ferraro, F. R., Pecci, F. F., Cacciari, C., et al. 1993, AJ, 106, 2324
Ferraro, F. R., Possenti, A., Sabbi, E., et al. 2003, ApJ, 595, 179
Ferraro, F. R., Sollima, A., Rood, R. T., et al. 2006a, ApJ, 638, 433
Fiorentino, G., Lanzoni, B., Dalessandro, E., et al. 2014, ApJ, 783, 34
Fisher, J., Schröder, K.-P., & Smith, R. C. 2005, MNRAS, 361, 495
Fitzgerald, M. T., Criss, J., Lukaszewicz, T., et al. 2012, PASA, 29, 72
Frank, M. J., Grebel, E. K., & K&uumlpper, A. H. W. 2014, MNRAS, 443, 815
Geisler, D., Piatti, A. E., Claria, J. J., & Minniti, D. 1995, AJ, 109, 605
Gilliland, R. L., Bono, G., Edmonds, P. D., et al. 1998, ApJ, 507, 818
Goldsbury, R., Richer, H. B., Anderson, J., et al. 2010, AJ, 140, 1830
Harris, W. E. 1996, AJ, 112, 1487
Heggie, D., & Hut, P. 2003, in The Gravitational Million-Body Problem: A Multidisciplinary Approach to Star Cluster Dynamics, ed. D. Heggie & P. Hut (Cambridge: Cambridge Univ. Press)

Heinke, C. O., Grindlay, J. E., Lugger, P. M., et al. 2003, ApJ, 598, 501
King, I. R. 1966, AJ, 71, 64
Kroupa, P. 2002, Science, 295, 82
Lanzoni, B., Dalessandro, E., Ferraro, F. R., et al. 2007a, ApJ, 663, 1040
Lanzoni, B., Dalessandro, E., Perina, S., et al. 2007b, ApJ, 670, 1065
Liller, M. H. 1981, AJ, 86, 1204
Mackey, A. D., & Gilmore, G. F. 2004, MNRAS, 355, 504
Mackey, A. D., & van den Bergh, S. 2005, MNRAS, 360, 631
Mapelli, M., Sigurdsson, S., Ferraro, F. R., et al. 2006b, MNRAS, 373, 361
Maraston, C. 1998, MNRAS, 300, 872
Marconi, G., Andreuzzi, G., Pulone, L., et al. 2001, A&A, 380, 478
Martin, N. F., Ibata, R. A., Bellazzini, M., et al. 2004, MNRAS, 348, 12
Mateo, M. 1996, ASP Conf. Ser. 90, The Origins, Evolution, and Destinies of Binary Stars in Clusters, ed. E. F. Milone & J. C. Mermilliod (San Francisco, CA: ASP), 21
Mathieu, R. D., & Geller, A. M. 2009, Natur, 462, 1032
McCrea, W. H. 1964, MNRAS, 128, 147
McLaughlin, D. E., & van der Marel, R. P. 2005, ApJS, 161, 304
Meylan, G., & Heggie, D. C. 1997, A&ARv, 8, 1
Milone, A. P., Piotto, G., Bedin, L. R., et al. 2012, A&A, 540, AA16
Miocchi, P., Lanzoni, B., Ferraro, F. R., et al. 2013, ApJ, 774, 151
Miocchi, P., Pasquato, M., Lanzoni, B., et al. 2015, ApJ, 799, 44
Moffat, A. F. J. 1969, A&A, 3, 455
Paresce, F., de Marchi, G., & Ferraro, F. R. 1992, Natur, 360, 46
Pooley, D., & Hut, P. 2006, ApJL, 646, L143
Renzini, A., & Fusi Pecci, F. 1988, ARA&A, 26, 199
Robin, A. C., Reylé, C., Derrière, S., & Picaud, S. 2003, A&A, 409, 523
Romani, R. W., & Weinberg, M. D. 1991, ApJ, 372, 487
Rutledge, G. A., Hesser, J. E., & Stetson, P. B. 1997, PASP, 109, 907
Salinas, R., Jílková, L., Carraro, G., Catelan, M., & Amigo, P. 2012, MNRAS, 421, 960
Sandage, A. 1962, ApJ, 135, 349
Sarajedini, A., Bedin, L. R., Chaboyer, B., et al. 2007, AJ, 133, 1658
Sarajedini, A., & Da Costa, G. S. 1991, AJ, 102, 628
Shara, M. M., Saffer, R. A., & Livio, M. 1997, ApJL, 489, L59
Sollima, A., Beccari, G., Ferraro, F. R., Fusi Pecci, F., & Sarajedini, A. 2007, MNRAS, 380, 781
Sollima, A., Martínez-Delgado, D., Valls-Gabaud, D., & Peñarrubia, J. 2011, ApJ, 726, 47
Spitzer, L. 1987, (Princeton, NJ: Princeton Univ. Press), 191
Spurzem, R. 2001, in Dynamics of Star Clusters and the Milky Way, Vol. 228, ed. S. Deiters et al. (San Francisco, CA: ASP), 75
Stetson, P. B. 1987, PASP, 99, 191
Stetson, P. B. 1994, PASP, 106, 250
Stetson, P. B. 2000, PASP, 112, 925
Tsuchiya, T., Korchagin, V. I., & Dinescu, D. I. 2004, MNRAS, 350, 1141
van den Bergh, S., & Mackey, A. D. 2004, MNRAS, 354, 713
Xin, Y., Ferraro, F. R., Lu, P., et al. 2015, ApJ, 801, 67